Title

A murine model of *Trypanosoma brucei*-induced myocarditis and cardiac dysfunction

Authors

Nathan P. Crilly[1,2], Marcelle Dina Zita[3], Alexander K. Beaver[1,2], Polina Sysa-Shah[1,4], Aashik Bhalodia[3], Kathy Gabrielson[1], Luigi Adamo[*3,] Monica R. Mugnier*[1,2]

*Co-Senior authors

Affiliations

[1] Department of Molecular and Comparative Pathobiology, School of Medicine, Johns Hopkins University, Baltimore, Maryland, USA

[2] Department of Molecular Microbiology and Immunology, Johns Hopkins Bloomberg School of Public Health, Baltimore, Maryland, USA

[3] Division of Cardiology, Department of Medicine, School of Medicine, Johns Hopkins University, Baltimore, Maryland, USA

[4] Molecular Imaging Service Center and Cancer Functional Imaging Core, School of Medicine, Johns Hopkins University, Baltimore, Maryland, USA

Corresponding authors

Monica R. Mugnier. mmugnie1@jhu.edu. 410-614-4894

Luigi Adamo. ladamo2@jhmi.edu

Conflict-of-interest statement

The authors have declared that no conflicts of interest exist

24 **Abstract**

25 *Trypanosoma brucei* is a protozoan parasite that causes human and animal African
26 trypanosomiases (HAT and AAT). Cardiac symptoms are commonly reported in HAT patients,
27 and intracardiac parasites with accompanying myocarditis have been observed in both natural
28 hosts and animal models of *T. brucei* infection. Despite the importance of *T. brucei* as a cause of
29 cardiac dysfunction and the dramatic socioeconomic impact of African trypanosomiases in sub-
30 Saharan Africa, there are currently no reproducible murine models of *T. brucei*-associated
31 cardiomyopathy. We present the first clinically relevant, reproducible murine model of cardiac
32 dysfunction in chronic *T. brucei* infection. Similar to humans, mice showed histological
33 evidence of myocarditis and elevation of serum NT-proBNP with electrocardiographic
34 abnormalities. Serum NT-proBNP levels were elevated prior to the development of severe
35 ventricular dysfunction. On flow cytometry, myocarditis was associated with an increase of most
36 myocardial immune cell populations, including multiple T cell and macrophage subsets,
37 corroborating the notion that *T. brucei*-associated cardiac damage is an immune-mediated event.
38 This novel mouse model represents a powerful and practical tool to investigate the pathogenesis
39 of *T. brucei*-mediated heart damage and supports the development of therapeutic options for *T.*
40 *brucei*-associated cardiac disease.

41

42

43

44 **Introduction**

45

46 The threat of *Trypanosoma brucei* is a fact of life throughout sub-Saharan Africa. A protozoan
47 parasite spread by the tsetse fly vector, *T. brucei* is the causative agent of two neglected tropical
48 diseases, human and animal African trypanosomiasis (HAT and AAT) (1). In both humans and
49 animals, the disease is characterized by waxing and waning fever followed by chronic wasting
50 and a coma which gives the disease its historical name, "sleeping sickness" (2, 3). Two
51 subspecies are responsible for human infection: *T. b. gambiense*, which is endemic in West and
52 Central Africa and *T. b. rhodesiense,* which is restricted to East and Southern Africa (4). The
53 disease character and progression are highly variable, although *T. b. rhodesiense* infection is
54 generally aggressive and rapidly progressive, while *T. b. gambiense* infection tends to follow a
55 more chronic, slowly progressive course (2). Although HAT is uncommon, with fewer than 1000
56 cases reported in 2019 through 2020, the ubiquity of animal reservoirs and the insect vector
57 throughout sub-Saharan Africa means that re-emergence is a constant threat (5–8). In addition to
58 the direct impacts on human health, AAT is a severe burden to animal agriculture throughout
59 sub-Saharan Africa and a serious contributor to food insecurity in the region, with an estimated
60 cost of $4.75 billion per year and an incalculable impact on individual livelihoods (9).

61

62 *T. brucei* is often thought of as a parasite of the hemolymphatics and central nervous system.
63 However, both historical and recent studies have led to a renewed appreciation for *T. brucei* as a
64 parasite of extravascular spaces (10, 11). *T. brucei* parasites invade and colonize multiple
65 extravascular tissues, including the heart, lungs, adipose tissue, skin, eyes, gonads, pancreas, and
66 brain (12, 13). Within these spaces, tissue-resident parasites are associated with widespread

67 inflammation and damage, resulting in loss of organ function that contributes to mortality (10,
68 11, 14).
69
70 *T. brucei* colonizes the heart, and cardiac disease is a likely contributor to HAT mortality (15,
71 16). HAT patients exhibit elevated cardiac NT-proBNP, a biomarker which is a sensitive
72 predictor of heart failure, and 19% report at least one symptom consistent with heart failure (16).
73 Although electrocardiography (ECG) is not routinely performed on HAT patients,
74 electrocardiographic abnormalities have been reported in up to 71% of HAT patients, with most
75 notable changes including prolonged QT interval and low voltage(16, 17). One study found that
76 patients in Cameroon with dilated cardiomyopathy were significantly more likely to have anti-
77 trypanosomal antibodies than healthy controls, suggesting that even clinically inapparent *T.*
78 *brucei* infection might contribute to cardiac dysfunction(18). In agreement with these clinical
79 findings, myocarditis has been reported in autopsies of patients who have died from HAT,
80 suggesting that cardiac inflammation is a contributor to *T. brucei*-associated cardiac disease (19,
81 20). Cardiac symptoms and resulting pathology have been reported in both *T. b. gambiense* and
82 *T. b. rhodesiense* infection (16). There is some evidence that *T. b. rhodesiense* causes more
83 severe cardiac pathology, but the small number of recorded cases make evaluation difficult (19,
84 21).
85
86 Unfortunately, while there is clear evidence that cardiac disease is a consequence of African
87 trypanosomiasis., *T. brucei*-associated heart disease remains understudied. In particular, there
88 has been a lack of well-established animal models to allow detailed investigation into the
89 pathology, pathogenesis, and functional consequences of *T. brucei*-associated heart disease.

90 Several historical studies have described the histopathology of myocarditis during *T. brucei*
91 infection, especially in large animal models such as cattle, dogs, and nonhuman primates (22–
92 25). While large animal models, especially primates, accurately recapitulate human disease, the
93 expense, difficulty, and ethical issues of working with such model species has prevented their
94 widespread adoption by *T. brucei* researchers. More recently, researchers have published a rat
95 model of acute cardiac disease during early *T. brucei* infection. In this acute model, infected rats
96 exhibited myocarditis and ventricular arrhythmias at 11 days postinfection (dpi), similar to the
97 pathological and EKG findings reported in human patients (16, 20, 26, 27). Although the rat
98 model demonstrates that *T. brucei*-related cardiac disease can be recapitulated in a rodent, there
99 are important limitations. Notably, studies in the rat have been limited to the first two weeks of
100 infection, while clinical data suggest that cardiac symptoms and myocarditis are most prominent
101 during chronic HAT (19, 20). In addition, studies in the rat model have been limited to analyzing
102 histopathology and ECG findings, although other modalities such as echocardiography and
103 measurement of cardiac biomarkers are important for assessing the severity and progression of
104 heart disease. Finally, there are relatively few tools for genetic and immunological manipulations
105 in the rat, potentially limiting its usefulness for investigating disease pathogenesis (28) .
106
107 A mouse model of *T. brucei*-associated cardiac disease would have multiple advantages.
108 Compared to other animal models, mice are relatively inexpensive, safe, and simple to handle
109 and house, making them practical for most investigators. In addition, there are numerous well-
110 characterized strains and knockout lines of mice, allowing detailed investigation into disease
111 mechanisms (28). Mice are also well-characterized as a model species for a variety of parasitic
112 diseases, including those caused by African (*T. brucei*) and New World (*Trypanosoma cruzi*)

113 trypanosomes (27, 28). Historical studies performed with infection protocols that cannot be
114 replicated in modern times showed evidence of myocarditis in *T. brucei*-infected mice via
115 histopathology, further supporting the utility of the mouse as a model of *T. brucei*-associated
116 cardiac disease, although the consequences of this inflammation were not evaluated (29, 30).
117 Overall, the establishment of a robust, reproducible mouse model would allow for a detailed
118 investigation into the mechanisms and consequences of *T. brucei*-associated cardiac disease and
119 would be instrumental to the development of novel therapeutic options.
120
121 In this study, we present the first reproducible, clinically relevant, murine model of African
122 Trypanosomiasis optimized to characterize the functional changes and immunology of *T. brucei*-
123 associated cardiac disease.
124

125 **Results**

126 ***T. brucei* infection in mice results in infection dynamics and clinical progression which are**
127 **comparable to HAT**

128 Trypanosomiasis can be induced in mice by injecting viable *T. brucei* parasites into the tail vein
129 of the mouse, resulting in a disease which is commonly used as a model for HAT (10, 31). To
130 demonstrate that the mouse model recapitulates major features of natural infection, we infected
131 adult male and female C57Bl/6J mice intravenously with 5-25 parasites of the *T. b. brucei*
132 subspecies, a non-human infective subspecies of *T. brucei* which is most closely related to *T. b.*
133 *rhodesiense* (4).
134

135 Following infection, parasitemia was measured every two days by hemocytometer. Parasitemia
136 first became detectable in the bloodstream at 4-6 dpi, and the first peak of parasitemia occurred
137 at 6-7 dpi (Fig 1A). At 8-10 dpi, the first trough of parasitemia occurred, when parasitemia
138 reached undetectable levels. For the remainder of infection, parasitemia fluctuated and was
139 highly variable between individual mice (Fig 1A).
140 *T. brucei* infection causes severe, multisystemic inflammation in natural hosts, with associated
141 splenomegaly (2, 32). To confirm that *T. brucei* infection caused systemic inflammation in our
142 model, mice were euthanized and the spleens were weighed at 28 dpi. Infected mice exhibited
143 significant splenomegaly, with a mean splenic weight of 466 g, compared to 80.1 g in age-
144 matched control mice (Fig 1B). Mice were euthanized when they reached 10^9 parasites per mL of
145 blood, lost >20% of body weight, or were assessed to be clinically terminal. Median survival
146 time was 39 dpi, with the first mouse reaching terminal endpoint at 31 dpi and the last surviving
147 until 49 dpi. Male mice exhibited a shorter survival time than female mice, although this
148 difference was not statistically significant (Supp. Fig 2.1A).
149
150 The dynamics of *T. brucei* infection in our model were in general agreement with other
151 published studies which have used similar mouse models and demonstrate that the mouse
152 recapitulates natural infection (10, 31, 33).
153
154 ***T. brucei* infection induces elevation in NT-ProBNP and ECG abnormalities prior to a**
155 **reduction in left ventricular ejection fraction**
156 At 28 days postinfection (dpi)—a commonly used timepoint to represent chronic *T. brucei*
157 infection—we evaluated cardiac biomarkers and function (31).

158

159 We measured cardiac NT-proBNP as a biomarker of cardiac dysfunction. Cardiac NT-proBNP is
160 a sensitive marker of heart failure (34). Released from cardiomyocytes under conditions of
161 excess stretch due to pressure or volume overload, NT-proBNP is elevated in HAT patients (16).
162 Plasma NT-proBNP concentrations were significantly increased in infected mice at 28 dpi (Fig.
163 2A). NT-proBNP levels were slightly more elevated in male than in female mice, although this
164 difference was not statistically significant (Supp. Fig. 2A).

165

166 We used echocardiography under sedation at 28 dpi to evaluate heart function. Infected mice had
167 significantly increased ejection fraction and fractional shortening at 28 dpi (Fig 2B). Ejection
168 fraction was slightly higher in infected males than in females, although this difference was not
169 statistically significant (Supp. Fig. 2B). To evaluate the cardiac conduction system, we used
170 ECG. Infected mice exhibited several ECG changes. As compared to uninfected controls,
171 infected animals had a lower heart rate. A review of the EKG tracings showed that this was due
172 both to a reduction in the intrinsic heart rate and to a significant burden of arrhythmias, including
173 grouped beating and dropped beats, with significantly elevated QT intervals, including when QT
174 interval was corrected for heart rate (QTc) (Fig. 2C). Overall, ECG findings were highly
175 suggested of AV node dysfunction and intermittent high-degree atrioventricular block. ECG
176 abnormalities were more exaggerated in infected males than females, although the differences
177 were not statistically significant (Supp. Fig. 2C). All measured ECG parameters are shown in
178 Table 1.

179

180 To further explore our observations, we repeated our functional assessments at 33 dpi, the latest
181 timepoint at which mice can be experimentally manipulated before they begin to succumb to
182 disease. Unsurprisingly, plasma NT-proBNP was again significantly elevated, with the mean
183 NT-proBNP concentration (173.5 pg/mL) being similar to that observed at 28 dpi (165.4 pg/mL)
184 (Fig. 3A). Due to the fragility of the mice at this timepoint, echocardiography was performed
185 awake. Even so, 2 male mice and 1 female mouse had to be excluded due to reaching terminal
186 endpoint before or during the echocardiographic evaluation. Interestingly, at 33 dpi mice
187 exhibited a decreased ejection fraction, opposite to what was seen at 28 dpi (Fig. 3B). This could
188 indicate cardiac decompensation as mice approach terminal status. It should be noted that, due to
189 the fragility of mice at 33 dpi, echocardiography was performed awake, a technique that typically
190 results in higher measured ejection fraction. Therefore, our findings indicate a significant drop in
191 cardiac contractility between 28 dpi and 33 dpi.
192

193 ***T. brucei* colonizes the myocardial interstitial space and causes myocarditis**

194 Within the mammalian host, parasites live extracellularly and colonize multiple extravascular
195 spaces, including the heart, ultimately causing fatal disease (13, 14). To confirm the presence of
196 intracardiac parasites in our model and to demonstrate that these parasites are extravascular, we
197 infected adult C57Bl/6J mice with genetically modified *T. brucei* parasites that constitutively
198 express the tdTomato fluorescent protein (35)(35). This parasite line has previously been shown
199 to exhibit similar infection dynamics as wild-type *T. brucei* parasites (13, 35). Mice were
200 sacrificed at 14 dpi, a timepoint when extravascular parasite populations have been established
201 and can be demonstrated on microscopy (10, 13). After sacrifice, we perfused mice to remove
202 intravascular parasites, collected the heart, and performed immunofluorescence for CD31 to

203 visualize the vasculature. *T. brucei* parasites were identified within the interstitial spaces of the
204 heart. Intracardiac parasites localized separately from CD31-lined spaces, indicating that
205 intracardiac parasites are extravascular (Fig 4, Supp. Fig 3).
206
207 To evaluate cardiac pathology due to *T. brucei* infection, we performed histopathology on the
208 hearts of 6 *T. brucei*-infected mice at 28 dpi. Of the 6 hearts evaluated, 5 met the Dallas Criteria
209 for lymphocytic myocarditis, while the sixth exhibited borderline myocarditis (36). To further
210 characterize histopathological changes, we used an established quantitative grading system to
211 evaluate the severity of myocarditis (Table 2) (37). At 28 dpi, all mice exhibited myocarditis,
212 with an average histological grade of 2, indicating moderate multifocal myocarditis (Fig 5A).
213 Inflammation affected all layers of the heart, including endocardium, myocardium, and
214 epicardium. On histopathology, observed cells included large numbers of lymphocytes, plasma
215 cells, and macrophages. Necrosis was not a major feature. The severity of inflammation was
216 most severe in the atria and at the atrioventricular (AV) junction (Fig 5B). The pattern and
217 severity of inflammation observed were consistent with previous histopathology findings in
218 humans and natural hosts (20, 22–25, 29, 38, 39). To evaluate cardiac fibrosis, longitudinal
219 sections of the heart were stained with Masson's Trichrome, and the percentage of collagen in
220 the myocardium was quantified using the Automated Fibrosis Analysis Tool (AFAT) (40). At 28
221 dpi, infected mice had a higher percentage of collagen in the heart compared to uninfected mice,
222 although this difference was not statistically significant (Fig 5C).
223
224 **Immune cell populations in the heart are consistent with immune-mediated myocarditis**

225 We had identified myocarditis as a consequence of *T. brucei* infection, and previous research has
226 indicated that the host immune response may contribute to *T. brucei*-associated cardiac
227 pathology (29). To better understand the intracardiac immune response to *T. brucei*, we
228 performed flow cytometry at 28 dpi to characterize the immune cell population in the heart.
229 Numbers of CD45+ cells/mg of tissue were markedly elevated in the hearts of all infected mice
230 at 28 dpi, supporting our histopathological finding of myocarditis (Fig 6A).
231
232 Examining individual cell populations, most immune cell lineages were more abundant in *T.*
233 *brucei* infected hearts than in age-matched controls (Fig 6B-C). In agreement with the functional
234 data, most immune cell populations were slightly more elevated in males than in females,
235 although the difference was not statistically significant for any cell lineage (Supp. Fig 2E-F).
236
237 Numbers of both CD4+ T cells and macrophages were significantly increased in infected hearts,
238 which is unsurprising, since these cell types are necessary for an effective immune response to
239 African trypanosomes (Fig 6B-C) (41). Of the different macrophage subsets, the CCR2^{hi}MHC-
240 II^{hi} population experienced the largest increase in numbers. This subset represents pro-
241 inflammatory, monocyte-derived macrophages, indicating that *T. brucei* infection causes an
242 influx of pro-inflammatory macrophages into the heart (42, 43). There was also a significant
243 elevation of both CD8+ T cells and natural killer (NK) cells, even though cell-mediated
244 immunity is relatively ineffective at responding to *T. brucei,* which is an extracellular parasite
245 (42, 43).
246
247

248 **Discussion**

249 *T. brucei*-associated cardiac disease is an underappreciated and understudied aspect of African
250 trypanosomiasis. Here we report a reproducible murine model of *T. brucei* infection optimized to
251 investigate acute and chronic *T. brucei*-associated cardiac disease. We demonstrate that this
252 model recapitulates key aspects of *T. brucei*-associated cardiac disease in humans and natural
253 hosts, including the presence of intracardiac parasites, myocarditis, EKG changes and elevated
254 NT-proBNP. Using this model, we learned that *T. brucei* infection results in parasite colonization
255 of the myocardial extracellular space and elevation of NT-proBNP (Figs 2-3). NT-proBNP
256 elevation was initially present in the context of a preserved ejection fraction, but the infection
257 eventually resulted in severe cardiac dysfunction as mice approached terminal endpoint (Figs 2-
258 3). At a histological level, we found that myocardial colonization by the parasite triggered a
259 severe myocarditis characterized by cardiomyocyte damage (Fig 5) and a multilineage
260 inflammatory infiltrate (Fig 6). These findings advance our understanding of the host-pathogen
261 interactions in the heart, suggesting that cardiac dysfunction associated with *T. brucei* infection
262 is an immune-mediated event, potentially providing valuable information to inform the
263 development of novel targeted therapies for animals and humans affected by African
264 trypanosomiases.

265

266 Animal models have been used to study *T. brucei* infection since the early 1900s, and the first
267 attempts to use a murine model to investigate *T. brucei*-associated cardiac disease were
268 published in the late 1970s (15, 29, 30) . In these historical murine studies, investigators
269 demonstrated cardiac lesions in infected mice and showed that immunosuppression was
270 associated with a reduction in the size and frequency of inflammatory cardiac lesions (29).

271 However, despite their seminal nature, these studies were limited in the scope of their
272 investigation, primarily focusing on histopathology and lacking more detailed functional or
273 immunological assessments. Moreover, the studies were performed using infection protocols and
274 parasite lines which were not standardized, thus making their methods challenging to replicate.
275 Our present work expands significantly on those historical studies as it presents a reproducible
276 method to generate cardiac damage and dysfunction in a murine model, demonstrably
277 recapitulating multiple aspects of natural disease.
278
279 We have found that mice infected with *T. brucei* initially exhibit elevation in NT-proBNP and
280 electrocardiographic abnormalities in the context of a preserved left ventricular ejection fraction.
281 At 28 dpi, when we initially assessed BNP, the mice had clear histological evidence of
282 myocarditis. NT-proBNP is elevated in response to an increase in intracardiac filling pressures
283 (34). In the context of a normal ejection fraction and cardiac pathology, BNP elevation is highly
284 suggestive of Heart Failure with Preserved Ejection fraction (HFpEF), a clinical condition
285 characterized by reduced cardiac performance and symptoms of heart failure despite a seemingly
286 normal cardiac contractility (44). However, BNP elevation in the context of a normal ejection
287 fraction has also been described in patients with acute myocarditis, likely as a result of stiffening
288 of cardiac walls triggered by the intracardiac immune response (45, 46). The potential overlap
289 between myocarditis with preserved ejection fraction and elevated BNP and HFpEF is an area
290 that has not been properly investigated so far in the clinical setting. However, taken together, our
291 findings suggest that colonization of the cardiac interstitium by *T. brucei* might result in a
292 stiffening of cardiac walls and elevation of cardiac pressures compatible with HFpEF, and that
293 the myocarditic immune response triggered by the parasites likely plays a key role in this

294 process. We hypothesize that as mice approach terminal endpoint, the cardiac pathology
295 becomes severe enough to cause a decrease in ejection fraction. However, more definite
296 conclusions require more detailed investigation into the functional impact of *T. brucei* infection
297 at multiple timepoints.
298
299 At 28 dpi, electrocardiographic abnormalities included marked bradycardia, increased QT
300 interval, grouped beating and dropped beats. These findings are in agreement with reports from
301 HAT patients, in which increased QT interval is the most common findings (16, 17). AV blocks
302 have also been reported in a subset of HAT patients, while autopsies have found inflammation of
303 the sinoatrial node, suggesting a disruption of the cardiac conduction system (47). Interestingly,
304 we did not observe premature ventricular contractions (PVCs), which have been observed in a rat
305 model of African trypanosomiasis (26). However, the relatively short recording period in our
306 study (1 minute per animal) may have hampered measurements of PVCs compared to the rat
307 model, in which 30-minute ECG recordings were analyzed (26).
308 We used flow cytometry to investigate the intracardiac immune milieu during *T. brucei*
309 infection. Previous studies in humans and large animal models have found that the major
310 immune effectors during *T. brucei* infection are B cells, CD4+ T cells, and macrophages, which
311 are all necessary for a protective anti-trypanosomal immune response (41). On the other hand,
312 CD8+ T cells and natural killer (NK) cells are thought to be mediators of pathological
313 inflammation in *T. brucei* infection, and their activation is associated with worse clinical
314 outcomes (41, 48, 49). In agreement with our histopathological finding of myocarditis, we found
315 that most intracardiac immune cell populations were elevated, especially CD4+ and CD8+ T
316 cells, macrophages, and NK cells. The most highly elevated macrophage subset was the

317 CCR2^{hi}MHC-II^{hi} population, which represents pro-inflammatory, monocyte-derived
318 macrophages (42, 43). Such pro-inflammatory macrophages are necessary for an effective
319 immune response to *T. brucei* (41). However, increased activation of anti-inflammatory,
320 alternatively-activated macrophages during chronic *T. brucei* infection is important for long-term
321 survival in experimentally infected animals, due to their ability to attenuate pathological
322 inflammation (47, 48). The large numbers of intracardiac CCR2^{hi}MHC-II^{hi} in our model suggests
323 that an imbalance between pro-inflammatory and anti-inflammatory macrophages could be a
324 contributor to myocarditis in our model. The elevation of CD8+ T cells and NK cells in the heart
325 are further suggestive of immunopathology as a contributor to cardiac damage. Increases in these
326 cell populations are suggestive of a response to intracellular antigens, although *T. brucei* is
327 entirely extracellular throughout its life cycle (48). Since CD8+ T cells are not a major feature of
328 the immune response to extracellular pathogens, we hypothesize that their elevation in our model
329 indicates a response to cardiac self-antigens, indicating an auto-immune component of the
330 observed myocarditis. This hypothesis is corroborated by other evidence suggesting that *T.*
331 *brucei*-associated organ damage has an auto-immune component. A recent study found that
332 meningeal B cells produce high-affinity autoantibodies during *T. brucei* infection, suggesting
333 that autoimmune responses may be a component of *T. brucei*-associated pathology in multiple
334 tissues(50). Clinically, cardiomyopathy patients in Cameroon have been found to have high
335 levels of both anti-trypanosomal and anti-heart antibodies, further indicating a connection
336 between *T. brucei* infection and autoimmune heart disease (18).
337
338 Furthermore, we hypothesize that immunopathology in the heart during *T. brucei* infection
339 follows a similar process to the pathogenesis of Chagas cardiomyopathy, caused by the New

340 World trypanosome *Trypanosoma cruzi.* The leading theory to explain the pathogenesis of
341 Chagas disease posits that parasite colonization of the heart induces inflammation and release of
342 self-antigens, resulting in a breakdown of self-tolerance and immune destruction of
343 cardiomyocytes (51). With chronicity, loss of cardiac muscle and replacement with scar tissue
344 causes a collapse in cardiac function, ultimately ending in the characteristic Chagas
345 cardiomyopathy (51). Our findings suggest that similar mechanisms might be at play during *T.*
346 *brucei* infection.
347
348 There was no increase in the B cell population in the heart. This is somewhat surprising, since
349 antibodies are the major mediators of immune clearance of *T. brucei*, and B cells are crucial for
350 systemic anti-trypanosomal immunity (41). However, our findings are consistent with other
351 tissue-specific flow cytometry experiments during *T. brucei* infection, which have identified no
352 changes in number of B cells in the lungs or adipose bodies of *T. brucei*-infected mice (14, 33).
353 In contrast, other models of myocarditis and heart failure show that intracardiac B cell
354 populations are increased and play a major pathologic role during viral myocarditis and
355 myocardial infarction (52–57). It is possible that B cell activation plays a role in *T. brucei*-
356 associated cardiac disease, even if there is no expansion of local populations.
357
358 We found limited evidence of a sex-specific difference in *T. brucei*-associated cardiac disease.
359 Male mice exhibited higher NT-proBNP at 33 dpi, higher numbers of intracardiac immune cells,
360 and more severe echocardiographic and ECG changes than females, although these differences
361 were not statistically significant. Our findings are in agreement with evidence that HAT is more
362 severe in men than women, as well as recent findings which indicate that T. brucei causes more

severe weight loss and adipose wasting in male rodents (58, 59). Our findings are also consistent with data indicating that myocarditis is more common in men than women (60). Further work will be needed to expand on these observations and dissect the mechanistic basis of sex differences in HAT.

Much about *T. brucei*-associated cardiac disease remains unknown, and there are serious gaps in our current knowledge, which this animal model could be used to investigate. Our findings raise concerns about long-term, post-treatment consequences of *T. brucei* infection. Most HAT patients are identified and treated, permanently clearing infection. However, the severity of the myocarditis reported by ourselves and others suggests that heart dysfunction might be only loosely connected with parasite presence. (20, 22–25, 29, 38, 39). If so, anti-parasitic treatment would not fully alleviate the cardiac symptoms of HAT, since self-directed inflammation could continue even with the removal of the inciting stimulus. Moreover, this suggests that immunomodulatory therapies could be considered for treatment of both humans and cattle to suppress inflammation that could contribute to persistent heart disease. There is a necessity to investigate the long-term and post-treatment consequences of *T. brucei*-associated myocarditis to determine whether HAT patients are at increased lifetime risk of heart failure. In addition, the effect of *T. brucei* subspecies on cardiac disease remains to be investigated. Our mouse model most closely recapitulates HAT due to *T. b. rhodesiense* infection. However, currently the majority of human cases are caused by *T. b. gambiense*, which often causes a disease of a more chronic character than *T. b. rhodesiense* (2). Although there is clinical evidence that all T. brucei subspecies cause cardiac disease, the differences in cardiac manifestations between subspecies are uncertain (16, 21, 61).

In summary, we describe the first reproducible, optimized, clinically relevant murine model of *T. brucei*-associated cardiac disease, a feature of African trypanosomiasis that is often overlooked in current textbooks and clinical resources. In the context of this model's characterization, we produced evidence suggesting that *T. brucei*-associated cardiac damage is an immune-mediated event. Future studies with this model will be instrumental in identifying potential treatments for cardiac manifestations of African trypanosomiasis, a disease which continues to take an extensive human and economic toll in large regions of the world.

Methods

Sex as a biological variable

409 For all experiments, data from both male and female mice were collected and analyzed.

410

411 **Mouse and parasite strains and infection**

412 Male and female C57Bl/6J mice (WT, strain# 000664 Jackson Laboratory) between 7-10 weeks
413 old were each infected by intravenous tail vein injection with ∼5 pleiomorphic EATRO 1125
414 AnTat1.1E 90-13 *T. brucei brucei* parasites. To quantify parasitemia, blood was collected from
415 the tail vein every two 2 days starting at 4 days post-infection (dpi), and parasites were counted
416 via hemocytometer (Supplemental Figure 1). Blood (125 uL) was collected by a submandibular
417 bleed at terminal endpoint (28 or 33 dpi). Unless otherwise described, mice were euthanized at
418 terminal endpoint by intraperitoneal injection of ketamine/xylazine and perfused with 50 mL of
419 PBS-Glucose (0.055M D-glucose) with heparin to remove intravascular parasites.

420

421 For immunofluorescence experiments, mice were infected intravenously with ~5 AnTat1.1E
422 chimeric triple reporter *T. brucei* parasites which express tdTomato (35). Parasitemia was
423 measured as previously described. At 14 dpi, mice were sacrificed as previously described.

424

425 For flow cytometry experiments, mice were infected and parasitemia was measured as
426 previously described. Mice were sacrificed at 28 dpi using CO2 euthanasia.

427

428

429

430 **Echocardiography**

431 At 28 dpi, echocardiography was performed on sedated mice by a blinded investigator using a
432 Vevo 2100 Ultrasound System (VisualSonics Inc.) as described previously (62).
433
434 At 33 dpi, echocardiography was performed on awake mice using a 40-MHz transducer
435 (VisualSonics Inc.) as described previously (63).
436
437 **Electrocardiography**
438 At 28 dpi, ECG was performed on unanesthetized mice as previously described (64). The entire
439 procedure was performed in approximately 1 minute per mouse using a PowerLab data
440 acquisition system (model ML866, ADInstruments, Colorado Springs, CO) and Animal Bio
441 Amp (model ML136, ADInstruments). ECG data were analyzed using LabChart software
442 (ADInstruments). The lead II tracings were used for analysis.
443
444 **Heart digestion**
445 Heart digestion was performed using a technique previously (65). Briefly, after sacrifice, mice
446 were perfused with 3 mL Hank's Balanced Salt Solution (HBSS). 60 mg of heart tissue was
447 placed in a 15 mL tube with 3 mL of HBSS. Digestion was performed for half an hour with 300
448 units of DNase I (Sigma-Aldrich), 625 units of collagenase II (Sigma-Aldrich), and 50 units of
449 hyaluronidase II (Sigma-Aldrich). After digestion, the tubes were centrifuged at 250xg for 5
450 minutes at 4 °C, the supernatant was removed, and the pellet was resuspended in 5 mL ACK
451 lysis buffer (Invitrogen) and incubated for 5 minutes at room temperature to remove red blood
452 cells. Suspended cells were passed through a 50 μm filter and then prepared for flow cytometry.
453

454 **Flow cytometry**

455 Flow cytometry was performed using a technique previously described (65). Cell suspensions
456 were labeled with fluorescently conjugated antibodies (Supplemental Table 1). FACS was
457 performed on an Aurora Spectral Flow Cytometer (Cytek) and analyses were performed using
458 FlowJo version 10.8.1 (Becton Dickinson).

459

460 **NT-proBNP ELISA**

461 At 28 and 33 dpi, plasma was collected from mice via cheek-bleeding. NT-proBNP plasma
462 levels were measured using the LS-F34395 Mouse NT-proBNP Sandwich ELISA Kit (LSBio)
463 according to the manufacturer's instructions.

464

465 **Histopathology**

466 For histopathology experiments, animals were infected and sacrificed at 28 dpi as previously
467 described. Hearts were placed in 10% neutral buffered formalin and fixed at room temperature
468 for 48 hours. The heart was cut in half longitudinally and sectioned by the Johns Hopkins
469 Oncology Tissue and Imaging Services Core. To evaluate inflammation, hearts were stained with
470 hematoxylin and eosin and imaged with 4x, 10x, and 40x objectives using a Nikon Eclipse E400
471 light microscope (Nikon). Cardiac lesions were graded by a blinded veterinary pathologist using
472 a previously established both the Dallas Criteria and a semiquantitative scoring system for
473 myocarditis in rodents (Table 2) (36, 37). Briefly, the severity and extent of lesions was graded
474 using a five-point system from 0 to 4. A zero score indicates no infiltration. A '1' score indicates
475 very limited focal distribution of myocardial lesions. A '2' score indicates multiple lesions. A '3'
476 score indicates multiple regions with confluence and extensive necrosis. A '4' score indicates

477 lesions affecting most of the observed tissue. Images were captured using an Excelis 4K camera
478 (Unitron) and processed using ImageJ v1.53 image analysis software (NIH). All methods
479 followed published guidelines for experimental pathology (66). To evaluate cardiac fibrosis,
480 additional longitudinal sections of hearts were stained with Masson's Trichrome and scanned at
481 200x magnification using an Axios Z.1 scanner (Zeiss). The percentage of collagen in each heart
482 section was quantified using the AFAT (40).
483
484 **Immunofluorescence**
485 For immunofluorescence experiments, 8-week-old female C57Bl/6J mice were infected
486 intravenously with 5 triple marker *T. brucei* parasites (35). At 14 dpi, mice were euthanized and
487 perfused as previously described. Heart was collected and fixed in 4% paraformaldehyde in PBS
488 for 12 hours at 4 □C. Post-fixation, tissues were sectioned longitudinally, frozen embedded in
489 O.C.T. Compound (Tissue-Tek), and cut using cryostat microtome into 10 μm sections by the
490 Johns Hopkins Oncology Tissue and Imaging Services Core.
491
492 The following antibodies were applied to sections: rat anti-mouse CD-31 (SCBT) followed by
493 goat anti-rat Alexa Fluor 488 (CST). Coverslips were mounted using ProLong Gold (Life
494 technologies). Tissues were imaged with 4x, 10x and 20x objectives using a Nikon Eclipse 90i
495 fluorescence microscope (Nikon) and X-Cite 120 fluorescent lamp (Excelitas) with an ORCA-
496 ER digital CCD camera (Hammamatsu) and ImageJ v1.53 image analysis software (NIH). Image
497 collection and analysis followed published guidelines for rigor and reproducibility in
498 immunofluorescence (67).
499

500 **Statistics**

501 Unless otherwise described, figures were generated and statistical analyses were performed using
502 the Tidyverse package in R version 4.2.3 (68).

503

504 **Study approval**

505 Animal experiments were performed with the approval of the IACUC of Johns Hopkins
506 University under protocol MO22H163

507

508 **Data availability**

509 Values for all data points in graphs are reported in the Supporting Data Values file.

510

511 **Author contributions**

512 NPC, MRM and LA conceptualized the study. NPC, MDC, AKB, PS, and KG conducted
513 experiments and acquired the data. NPC, MDC, AL, PS, AB, and KG analyzed the data. KG,
514 LA, and MRM provided resources. NC wrote the original draft of the manuscript. NPC, AKB,
515 LA, and MRM reviewed and edited the manuscript. MRM acquired funding. MRM and LA
516 supervised the study.

517

518

519

520

521

522 **Acknowledgements**

523 We would like to kindly thank Brice Rotureau for providing us with the chimeric triple reporter
524 cell line.

525

526 The Aurora Flow Cytometer used in this study was funded by NIH Grant S10OD026859. We
527 acknowledge the support of the JHU Ross Flow Cytometry Core.

528

529 Echocardiograms were performed by Nadan Wang of the JHU Small Animal Cardiovascular
530 Phenotyping and Animal Model Core.

531

532 Histology support was provided by the JHU Oncology Tissue Services Core, funded by JHU
533 Cancer Center Core Grant P30 CA006973.

534

535 This project was supported by the Johns Hopkins Specialized Center for Research Excellence in
536 Sex Differences (U54AG062333) and The Foundation for Gender-Specific Medicine. NPC was
537 supported by T32 OD011089.

538

539

540

541

542

543

544

545 **References**

546 1. Holmes P. Tsetse-transmitted trypanosomes - Their biology, disease impact and control
547 [preprint]. *J Invertebr Pathol*. 2013;112(SUPPL.1). https://doi.org/10.1016/j.jip.2012.07.014.
548 2. Kennedy PGE, Rodgers J. Clinical and neuropathogenetic aspects of human African
549 trypanosomiasis [preprint]. *Front Immunol*. 2019;10(JAN).
550 https://doi.org/10.3389/fimmu.2019.00039.
551 3. Spickler AR. African Animal Trypanosomiasis [Internet]. *IO State University Center for Food*
552 *Security and Public Health*. 2018.
553 4. Balmer O, et al. Phylogeography and taxonomy of Trypanosoma brucei. *PLoS Negl Trop Dis*.
554 2011;5(2):e961.
555 5. Franco JR, et al. The elimination of human African trypanosomiasis: Achievements in relation
556 to WHO road map targets for 2020. *PLoS Negl Trop Dis*. 2022;16(1).
557 https://doi.org/10.1371/JOURNAL.PNTD.0010047.
558 6. Funk S, et al. Identifying Transmission Cycles at the Human-Animal Interface: The Role of
559 Animal Reservoirs in Maintaining Gambiense Human African Trypanosomiasis. *PLoS Comput*
560 *Biol*. 2013;9(1). https://doi.org/10.1371/journal.pcbi.1002855.
561 7. Njiokou F, et al. Wild fauna as a probable animal reservoir for Trypanosoma brucei gambiense
562 in Cameroon. *Infection, Genetics and Evolution*. 2006;6(2):147–153.
563 8. Njiokou F, et al. Domestic animals as potential reservoir hosts of Trypanosoma brucei
564 gambiense in sleeping sickness foci in Cameroon. *Parasite*. 2010;17(1):61–6.
565 9. Abro Z, et al. The potential economic benefits of controlling trypanosomiasis using waterbuck
566 repellent blend in sub-Saharan Africa. *PLoS One*. 2021;16(7 July).
567 https://doi.org/10.1371/journal.pone.0254558.
568 10. Trindade S, et al. Trypanosoma brucei Parasites Occupy and Functionally Adapt to the
569 Adipose Tissue in Mice. *Cell Host Microbe*. 2016;19(6):837–848.
570 11. Poltera AA. Pathology of human African trypanosomiasis with reference to experimental
571 African trypanosomiasis and infections of the central nervous system. *Br Med Bull*.
572 1985;41(2):169–174.
573 12. Crilly NP, Mugnier MR. Thinking outside the blood: Perspectives on tissue-resident
574 Trypanosoma brucei [preprint]. *PLoS Pathog*. 2021;17(9).
575 https://doi.org/10.1371/journal.ppat.1009866.
576 13. De Niz M, et al. Organotypic endothelial adhesion molecules are key for Trypanosoma
577 brucei tropism and virulence. *Cell Rep*. 2021;36(12).
578 https://doi.org/10.1016/j.celrep.2021.109741.
579 14. Machado H, et al. Trypanosoma brucei triggers a broad immune response in the adipose
580 tissue. *PLoS Pathog*. 2021;17(9). https://doi.org/10.1371/journal.ppat.1009933.
581 15. Wolbach SB, Binger CA. A Contribution to the Parasitology of Trypanosomiasis. *J Med Res*.
582 1912;27(1):83-108.13.
583 16. Blum JA, et al. Sleeping hearts: The role of the heart in sleeping sickness (human African
584 trypanosomiasis). *Tropical Medicine and International Health*. 2007;12(12):1422–1432.
585 17. Blum JA, et al. Cardiac alterations in human African trypanosomiasis (T.b. gambionse) with
586 respect to the disease stage and antiparasitic treatment. *PLoS Negl Trop Dis*. 2009;3(2).
587 https://doi.org/10.1371/journal.pntd.0000383.

588 18. Tsala Mbala P, et al. [Functional and immunologic involvement in human African
589 trypanosomiasis caused by Trypanosoma gambiense]. *Bull Soc Pathol Exot Filiales*. 1988;81(3
590 BIS):490–501.
591 19. Hawking F, Greenfield JG. Two autopsies on rhodesiense sleeping sickness; Visceral lesions
592 and significance of changes in cerebrospinal fluid. *Trans R Soc Trop Med Hyg*. 1941;35(3):155–
593 156.
594 20. Poltera AA, Cox JN, Owor R. Pancarditis affecting the conducting system and all valves in
595 human African trypanosomiasis. *Heart*. 1976;38(8):827–837.
596 21. Koten JW, de Raadt P. Myocarditis in Trypanosoma rhodesiense infections. *Trans R Soc*
597 *Trop Med Hyg*. 1969;63(4):485–489.
598 22. Poltera AA, et al. Trypanosomal cardiac valvulitis in vervet monkeys. *Tropical Medicine and*
599 *Parasitology*. 1985;36(2):77–80.
600 23. Ikede BO, Losos GJ. Pathology of the disease in sheep produced experimentally by
601 Trypanosoma brucei. *Vet Pathol*. 1972;9(4):278–289.
602 24. Ikede BO, Losos GJ. Pathological changes in cattle infected with Trypanosoma brucei. *Vet*
603 *Pathol*. 1972;9(4):272–277.
604 25. Morrison WI, et al. The pathogenesis of experimentally induced Trypanosoma brucei
605 infection in the dog I. Tissue and organ damage. *American Journal of Pathology*.
606 1981;102(2):168–181.
607 26. McCarroll CS, et al. A Pre-clinical Animal Model of Trypanosoma brucei Infection
608 Demonstrating Cardiac Dysfunction. *PLoS Negl Trop Dis*. 2015;9(5).
609 https://doi.org/10.1371/journal.pntd.0003811.
610 27. Elliott EB, et al. Trypanosoma brucei cathepsin-L increases arrhythmogenic sarcoplasmic
611 reticulum-mediated calcium release in rat cardiomyocytes. *Cardiovasc Res*. 2013;100(2):325–
612 335.
613 28. Wildner G. Are rats more human than mice? *Immunobiology*. 2019;224(1):172–176.
614 29. Poltera AA, Hochmann A, Lambert PH. A model for cardiopathy induced by Trypanosoma
615 brucei brucei in mice. A histologic and immunopathologic study. *American Journal of*
616 *Pathology*. 1980;99(2):325–352.
617 30. Galvao-Castro B, Hochmann A, Lambert PH. The role of the host immune response in the
618 development of tissue lesions associated with African trypanosomiasis in mice. *Clin Exp*
619 *Immunol*. 1978;33(1):12–24.
620 31. Beaver AK, et al. Extravascular spaces are the primary reservoir of antigenic diversity in
621 Trypanosoma brucei infection. *bioRxiv*. 2023;2022.06.27.497797.
622 32. Spickler AR. African Animal Trypanosomiasis [Internet]. 2018;2020.
623 http://www.cfsph.iastate.edu/DiseaseInfo/factsheets.php.
624 33. Mabille D, et al. Impact of pulmonary African trypanosomes on the immunology and
625 function of the lung. *Nat Commun*. 2022;13(1). https://doi.org/10.1038/s41467-022-34757-w.
626 34. Yancy CW, et al. 2017 ACC/AHA/HFSA Focused Update of the 2013 ACCF/AHA
627 Guideline for the Management of Heart Failure: A Report of the American College of
628 Cardiology/American Heart Association Task Force on Clinical Practice Guidelines and the
629 Heart Failure Society of America. *J Am Coll Cardiol*. 2017;70(6):776–803.
630 35. Calvo-Alvarez E, et al. A new chimeric triple reporter fusion protein as a tool for in vitro and
631 in vivo multimodal imaging to monitor the development of African trypanosomes and
632 Leishmania parasites. *Infection, Genetics and Evolution*. 2018;63:391–403.
633 36. Thomas Aretz H. Myocarditis: The Dallas criteria. *Hum Pathol*. 1987;18(6):619–624.

634 37. Aly M, et al. Complex genetic control of host susceptibility to coxsackievirus B3-induced
635 myocarditis. *Genes Immun*. 2007;8(3):193–204.
636 38. Dupont B, Charmot G, Lapresle C. [Trypanosomiasis presenting with trypanids and
637 complicated by myopericarditis (author's transl)]. *Nouv Presse Med*. 1979;8(19):1579–81.
638 39. Büngener W, Mehlitz D. [Experimental Trypanosoma infections in Cameroon dwarf goats:
639 histopathological observations (author's transl)]. *Tropenmed Parasitol*. 1976;27(4):405–10.
640 40. Gratz D, et al. Computational tools for automated histological image analysis and
641 quantification in cardiac tissue. *MethodsX*. 2020;7:22–34.
642 41. Onyilagha C, Uzonna JE. Host Immune Responses and Immune Evasion Strategies in
643 African Trypanosomiasis [preprint]. *Front Immunol*. 2019;10.
644 https://doi.org/10.3389/fimmu.2019.02738.
645 42. Dick SA, et al. Self-renewing resident cardiac macrophages limit adverse remodeling
646 following myocardial infarction. *Nat Immunol*. 2019;20(1):29–39.
647 43. Cohen CD, et al. Myocardial Immune Cells: The Basis of Cardiac Immunology. *The Journal*
648 *of Immunology*. 2023;210(9):1198–1207.
649 44. Ranek M, et al. Pathophysiology of heart failure and an overview of therapies. In: Buja L,
650 Butany J, eds. *Cardiovascular Pathology*. London: Academic Press; .
651 45. Sara B, et al. Are high NT-proBNP levels more related to inflammation than to left
652 ventricular systolic dysfunction in acute myocarditis? *Eur Heart J Acute Cardiovasc Care*.
653 2021;10(Supplement_1). https://doi.org/10.1093/ehjacc/zuab020.189.
654 46. Moady G, Perlmutter S, Atar S. The Prognostic Value of Natriuretic Peptides in Stable
655 Patients with Suspected Acute Myocarditis: A Retrospective Study. *J Clin Med*.
656 2022;11(9):2472.
657 47. Bertrand E, et al. La symptomatologie cardio-vasculaire dans la trypanosomiase humaine
658 Africaine a Trypanosoma gambiense.
659 48. Liu G, et al. Distinct contributions of CD4+ and CD8+ T cells to pathogenesis of
660 trypanosoma brucei infection in the context of gamma interferon and interleukin-10. *Infect*
661 *Immun*. 2015;83(7):2785–2795.
662 49. Frenkel D, et al. Trypanosoma brucei Co-opts NK Cells to Kill Splenic B2 B Cells. *PLoS*
663 *Pathog*. 2016;12(7). https://doi.org/10.1371/journal.ppat.1005733.
664 50. Quintana JF, et al. The murine meninges acquire lymphoid tissue properties and harbour
665 autoreactive B cells during chronic Trypanosoma brucei infection. *bioRxiv*.
666 2023;2023.04.30.538710.
667 51. Bonney KM, Engman DM. Autoimmune pathogenesis of chagas heart disease: Looking
668 back, looking ahead [preprint]. *American Journal of Pathology*. 2015;185(6):1537–1547.
669 52. Zouggari Y, et al. B lymphocytes trigger monocyte mobilization and impair heart function
670 after acute myocardial infarction. *Nat Med*. 2013;19(10):1273–1280.
671 53. Tschöpe C, et al. Myocarditis and inflammatory cardiomyopathy: current evidence and future
672 directions [preprint]. *Nat Rev Cardiol*. 2021;18(3):169–193.
673 54. Tschöpe C, et al. Targeting CD20+ B-lymphocytes in inflammatory dilated cardiomyopathy
674 with rituximab improves clinical course: a case series. *Eur Heart J Case Rep*. 2019;3(3).
675 https://doi.org/10.1093/ehjcr/ytz131.
676 55. Mo F, et al. Are activated B cells involved in the process of myocardial fibrosis after acute
677 myocardial infarction? An in vivo experiment. *BMC Cardiovasc Disord*. 2021;21(1).
678 https://doi.org/10.1186/s12872-020-01775-9.

56. Bermea K, et al. The Role of B Cells in Cardiomyopathy and Heart Failure [preprint]. *Curr Cardiol Rep*. 2022;24(8):935–946.
57. Adamo L, et al. Modulation of subsets of cardiac B lymphocytes improves cardiac function after acute injury. *JCI Insight*. 2018;3(11). https://doi.org/10.1172/jci.insight.120137.
58. Sinton MC, et al. IL-17 signalling is critical for controlling subcutaneous adipose tissue dynamics and parasite burden during chronic murine Trypanosoma brucei infection. *Nat Commun*. 2023;14(1). https://doi.org/10.1038/s41467-023-42918-8.
59. Pépin J, Mpia B, Iloasebe M. Trypanosoma brucei gambiense African trypanosomiasis: Differences between men and women in severity of disease and response to treatment. *Trans R Soc Trop Med Hyg*. 2002;96(4):421–426.
60. Fairweather DL, et al. Sex and gender differences in myocarditis and dilated cardiomyopathy: An update [preprint]. *Front Cardiovasc Med*. 2023;10. https://doi.org/10.3389/fcvm.2023.1129348.
61. Losos GJ, Ikede BO. Review of pathology of diseases in domestic and laboratory animals caused by Trypanosoma congolense, T. vivax, T. brucei, T. rhodesiense and T. gambiense. *Vet Pathol*. 1972;Sup. 9. https://doi.org/10.1177/030098587200901s01.
62. Fitch ML, et al. Cadmium exposure induces a sex-dependent decline in left ventricular cardiac function. *Life Sci*. 2023;324. https://doi.org/10.1016/j.lfs.2023.121712.
63. Sørensen LL, et al. Echocardiographic characterization of a murine model of hypertrophic obstructive cardiomyopathy induced by cardiac-specific overexpression of epidermal growth factor receptor 2. *Comp Med*. 2016;66(4):268–277.
64. Sysa-Shah P, et al. Electrocardiographic characterization of cardiac hypertrophy in mice that overexpress the ErbB2 receptor tyrosine kinase. *Comp Med*. 2015;65(4):295–307.
65. Bermea KC, Rousseau ST, Adamo L. Flow Cytometry-Based Quantification and Analysis of Myocardial B-cells. *Journal of Visualized Experiments*. 2022;2022(186). https://doi.org/10.3791/64344.
66. Scudamore CL, et al. Recommendations for minimum information for publication of experimental pathology data: MINPEPA guidelines [preprint]. *Journal of Pathology*. 2016;238(2):359–367.
67. Lee JY, Kitaoka M. A beginner's guide to rigor and reproducibility in fluorescence imaging experiments [preprint]. *Mol Biol Cell*. 2018;29(13):1519–1525.
68. Wickham H, et al. Welcome to the Tidyverse. *J Open Source Softw*. 2019;4(43):1686.

718 **Figures**

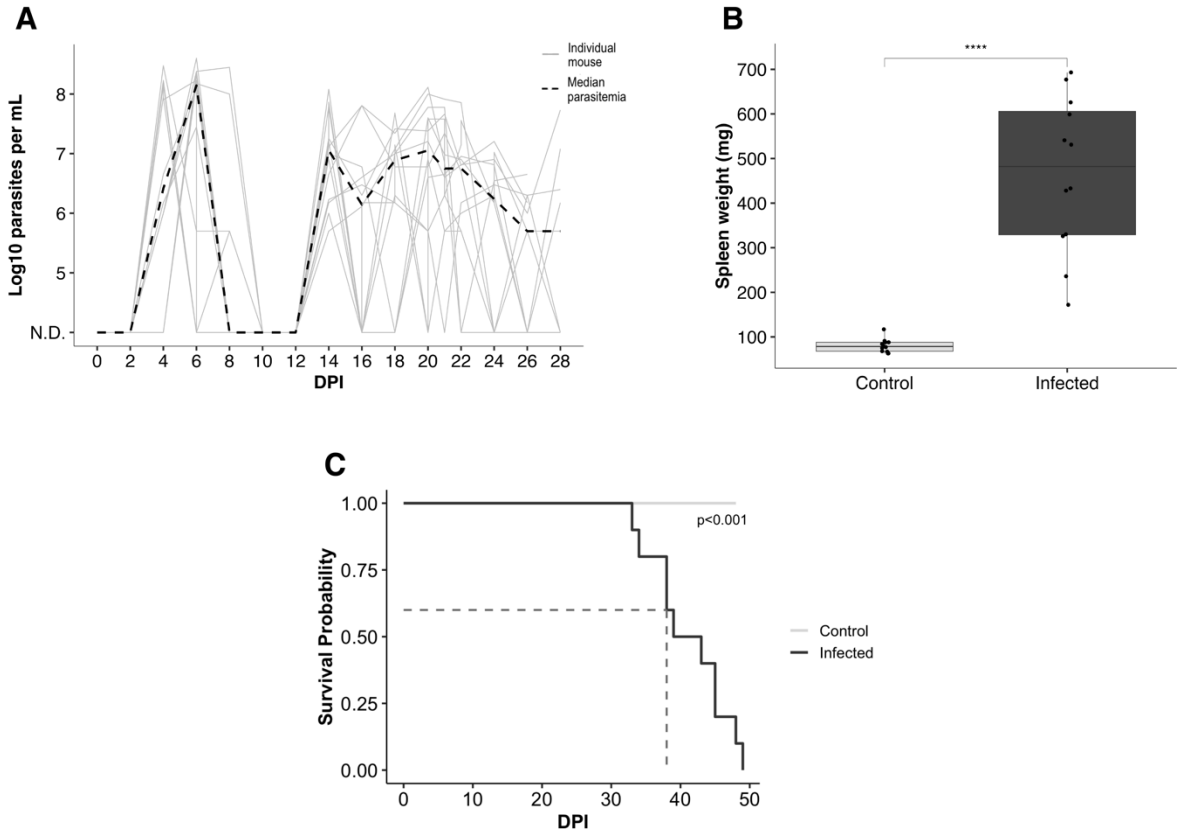

719

720 **Figure 1**. *T. brucei* infection causes waxing and waning waves of parasitemia and massive

721 splenomegaly, with terminal endpoint reached within 50 dpi

722 A. Quantification of median and individual parasitemia in a representative experiment.

723 Parasitemia first becomes detectable at 4-6 dpi.

724 B. Weight of spleens of infected mice at 28 dpi(n=6) compared to uninfected, age-matched

725 controls. Infected mice exhibit significant splenomegaly (Student's t-test, p=3.7E-06).

726 C. Kaplan-Meier survival curve of mice infected with T. brucei vs. uninfected control

727 animals. Infected mice have a median survival time=39 dpi (p=4.32E-05).

728

729

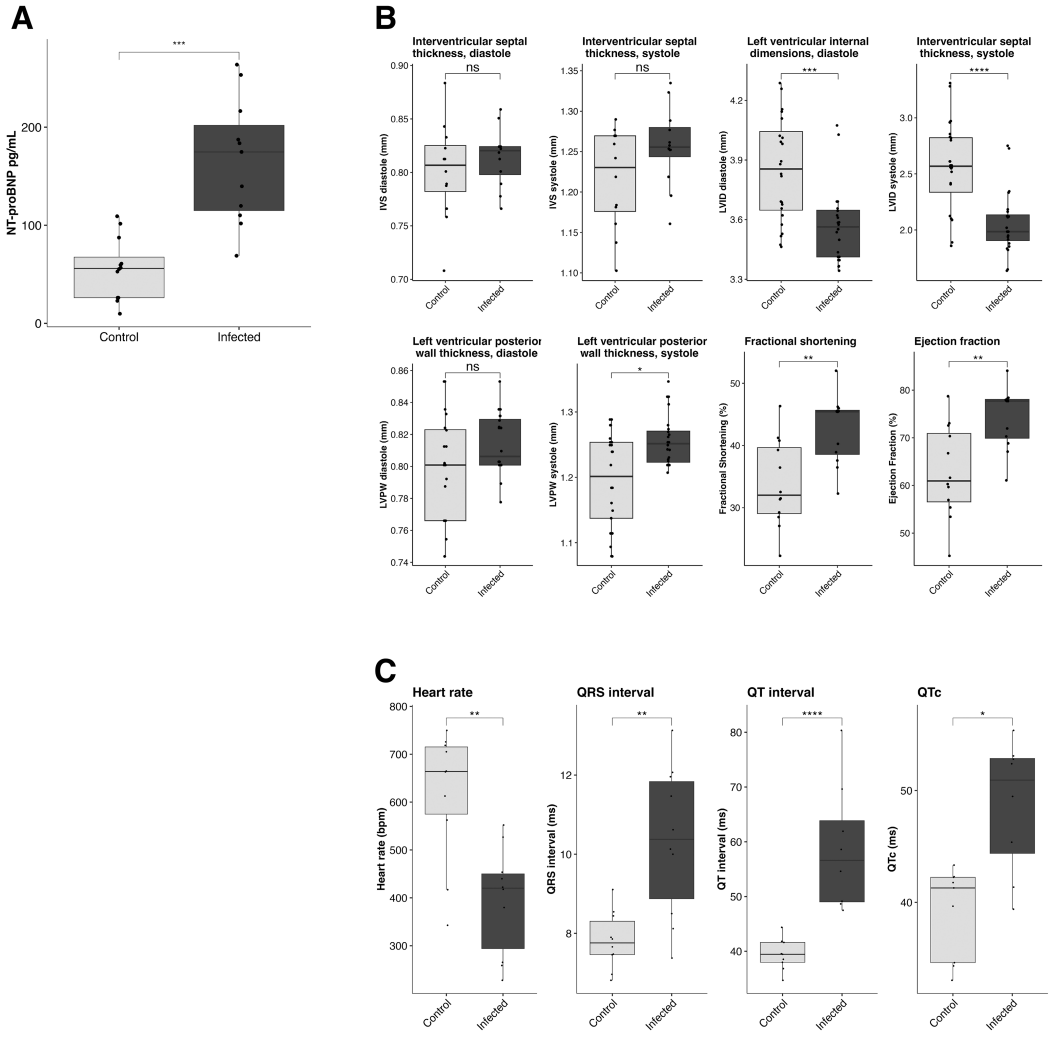

730

731 **Figure 2**. *T. brucei* infection causes elevated NT-proBNP, electrocardiographic abnormalities

732 and heart failure with preserved ejection fraction

733 A. Measurement of plasma NT-proBNP at 28 dpi. Plasma NT-proBNP is significantly

734 elevated at 28 dpi (n=12) compared to age-matched uninfected controls (Student's t-test,

735 p=0.00037).

736 B. Echocardiographic measurements at 28 dpi. At 28 dpi, infected mice (n=12) exhibit

737 significantly increased ejection fraction compared to uninfected age-matched controls, as

738 measured by sedated echocardiography (Student's t-test, p=0.0029).

739 C. Electrocardiographic measurements at 28 dpi. At 28 dpi, infected mice (n=10) exhibit
740 significantly decreased heart rate (HR, Student's t-test, p= 0.00011), increased QRS
741 interval, (Student's t-test, p=0.00281), increased QT interval (Student's t-test,
742 p=0.00493), and increased QTc (Student's t-test, p=0.01294) compared to uninfected
743 age-matched controls.
744
745
746
747
748
749
750
751
752

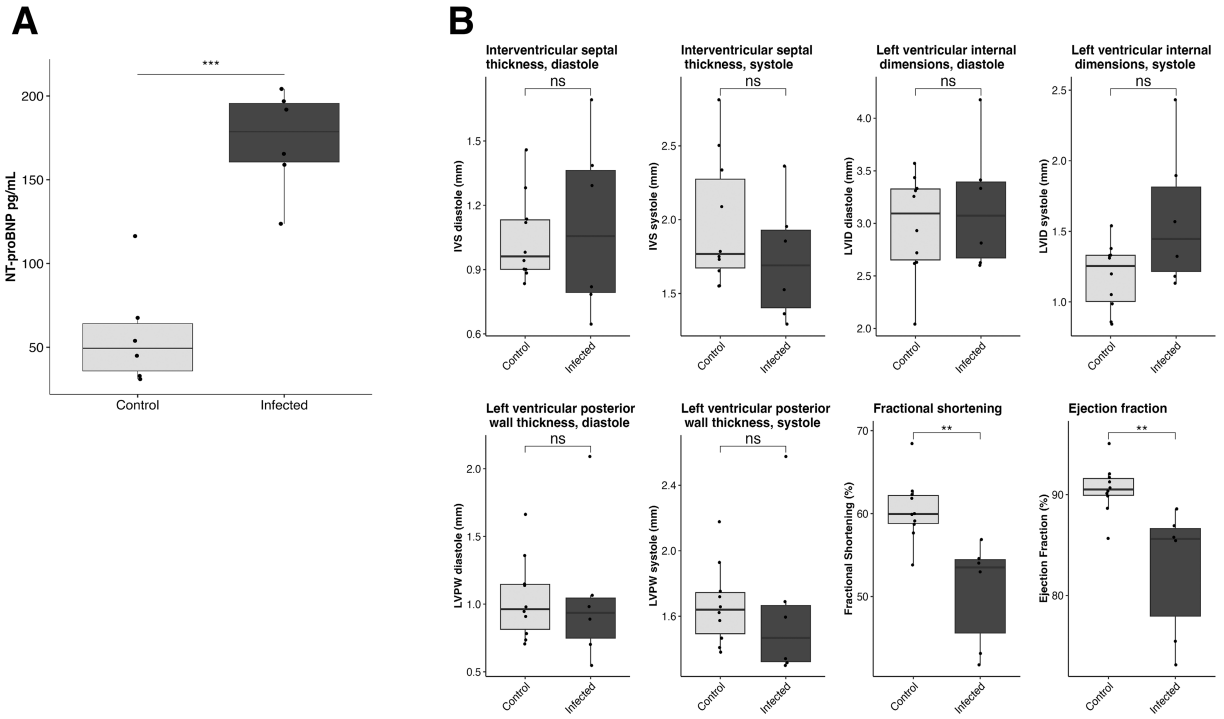

Figure 3. T. brucei infection causes elevated NT-proBNP and decreased heart function at terminal endpoint (33 dpi).

A. Measurement of plasma NT-proBNP at 33 dpi. Plasma NT-proBNP is significantly elevated at 33 dpi in infected mice (n=6) compared to uninfected age-matched controls (Student's t-test, p=2.8e-05).

B. Echocardiographic measurements at 33 dpi. At 33 dpi, infected mice (n=6) exhibit significantly decreased ejection fraction compared to uninfected age-matched controls, as measured by awake echocardiography (Student's t-test, p=0.011)

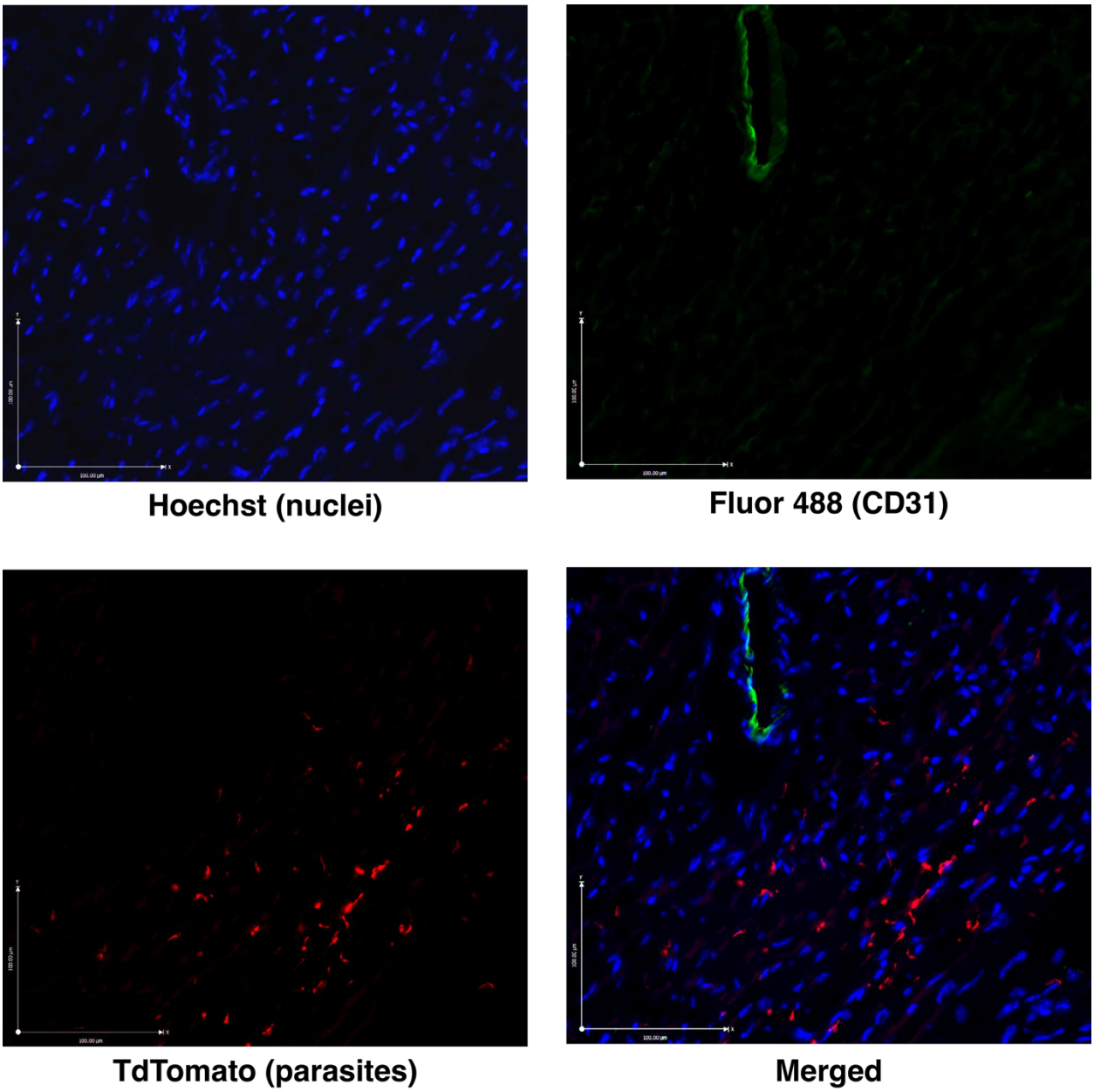

Figure 4. *T. brucei* parasites occupy extravascular spaces in the heart

Representative immunofluorescence microphotographs of the cardiac ventricle at 14 dpi at 20x magnification. *T. brucei* parasites (tdTomato—red) localize separately from CD31-lined vascular structures (Alexa Fluor 488—green), confirming the extravascular localization of parasites. Nuclei are stained with Hoechst (blue).

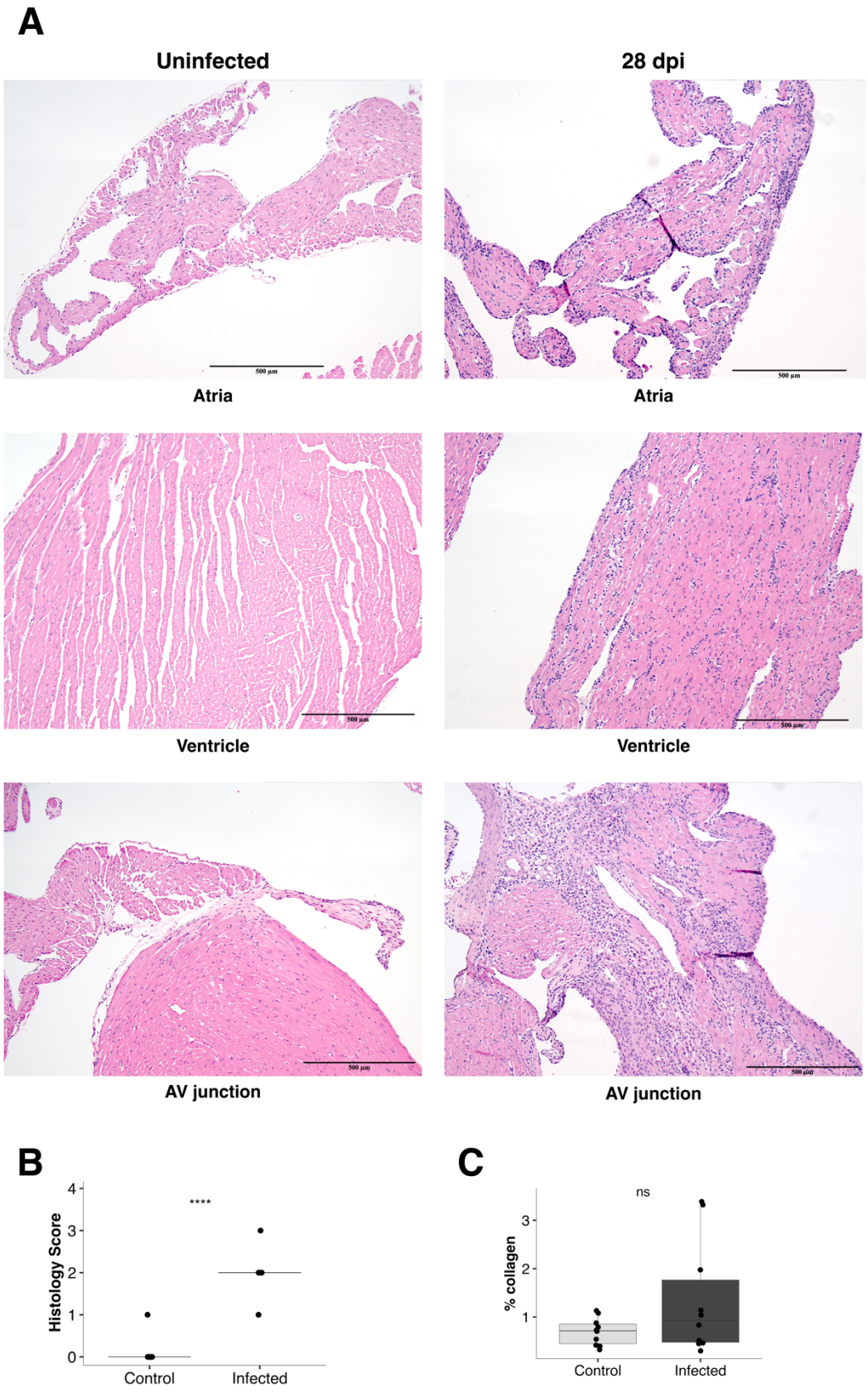
A
Uninfected
28 dpi
Atria
Atria
Ventricle
Ventricle
AV junction
AV junction
B
Histology Score
****
Control
Infected
C
% collagen
ns
Control
Infected

774

775 **Figure 5.** *T. brucei* infection causes myocarditis at 28 dpi

776 A. Representative brightfield microphotographs of the heart of infected mice at 28 dpi,
777 compared to uninfected age-matched controls at 10x magnification. Inflammation is
778 present in all layers and regions of the heart and is composed largely of mononuclear
779 cells, primarily lymphocytes, plasma cells, and histiocytes. Inflammation is most severe
780 at the atrioventricular junction.

781 B. Histological grading of myocarditis (n=6) at 28 dpi, compared to equal numbers of age-
782 matched controls. The average grade at 28 dpi is '2', indicating multifocal moderate
783 myocarditis without extensive associated necrosis. Histological grade is significantly
784 higher in infected than uninfected mice (Student's t test, p=1.5e-8).

785 C. Measurement of the percentage of collagen in longitudinal sections of heart (n=6) at 28
786 dpi, compared to equal numbers of age-matched controls. There is no significant
787 difference between infected and control mice (Student's t test, p=0.31).

788

789

790

791

792

793

794

795

796

797

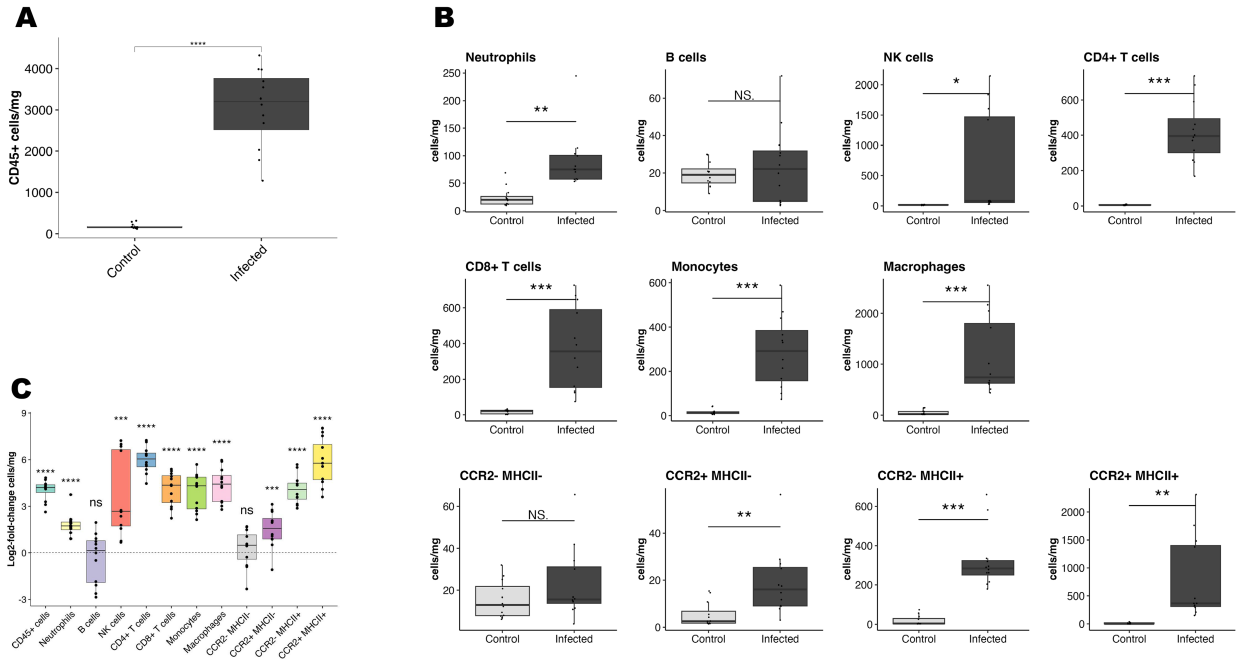

Figure 6. The intracardiac immune cell population during *T. brucei* infection is characteristic of immune-mediated myocarditis

A. Flow cytometric quantification of CD45+ cells per mg. At 28 dpi, CD45+ cells are markedly increased in the hearts of infected mice (n=12) compared to uninfected age-matched controls, supportive of myocarditis (Student's t-test, p= 4.6e-7).

B. Flow cytometric quantification of myeloid and lymphoid cell populations. Most immune cell populations are significantly increased in the hearts of infected mice at 28 dpi. Statistical comparisons were made using One-way Anova. *p<0.05, **p<0.01, ***p<0.001.

C. Visualization of magnitude of changes in immune cell populations using the log2-fold change in cells/mg compared to uninfected age-matched control mice calculated based on the average cells/mg in the hearts of uninfected control mice.

813 **Tables**

814

815 **Table 1:** Comparison of the mean values of all ECG parameters between infected animals and

816 age-matched controls at 28 dpi (NS, P>0.05. *, P ≤0.05. **, P ≤0.01. ***,P ≤0.001)

	Control	Infected	P value	Significance
RR Interval (ms)	104.98	166.77	0.00111	**
Heart Rate (BPM)	616.18	394.40	0.00011	***
QRS Interval (ms)	7.82	10.34	0.00281	**
QT Interval (ms)	39.43	58.80	0.00493	***
QTc (ms)	39.17	48.66	0.01294	*
JT Interval (ms)	31.77	48.25	0.00758	**
Tpeak Tend Interval (ms)	28.97	42.24	0.00985	**
Q Amplitude (mV)	0.01	0.02	0.42396	NS
R Amplitude (mV)	0.89	0.78	0.19872	NS
S Amplitude (mV)	-0.52	-0.30	0.00438	**
ST Height (mV)	0.10	0.07	0.32718	NS
T Amplitude (mV)	0.19	0.11	0.00670	**

817
818 NS, P>0.05. *, P ≤0.05. **, P ≤0.01. ***,P ≤0.001
819
820
821
822 **Table 2**: Histological grading criteria
823

Grade	Description
0	No inflammatory infiltrates
1	Limited focal distribution of myocardial lesions
2	Multiple lesions with inflammatory infiltrates and some confluence
3	Multiple lesions with confluence and extensive necrosis
4	Lesions affecting most of the observed tissue

824
825
826
827
828
829
830
831
832
833

Supplemental Materials

Supplemental data is available in the associated Supplemental Data document

Supporting data values are available in the associated Supporting Data Values document